crystals

MDPI

Article

Preparation and Structural Variety of Neutral Heptaphospha-Nortricyclane Derivatives of Zinc and the Coinage Metals

Clara A. Roller †, Berenike Doler † and Roland C. Fischer *

Institute of Inorganic Chemistry, Graz University of Technology, Stremayrgasse 9/V, 8010 Graz, Austria; c.roller@tugraz.at (C.A.R.)

* Correspondence: roland.fischer@tugraz.at

† These authors contributed equally to this work.

Abstract: In this study, we report the preparation of neutral Au(I), Ag(I), and Cu(I) derivatives $[(hyp)_2P_7M]_n$ (M = Au, n = 2; M = Ag, Cu, n = 4) of a heptaphospha-nortricyclane cage. Synthesis was conducted *via* a halodesilylation route under the cleavage of the sterically less shielded trimethyl silyl group, starting from the heteroleptic cage $(hyp)_2(tms)P_7$. All coinage metal derivatives exhibit short metal–metal distances of 2.9542(2) Å (Au), 2.8833(6) Å (Ag), and 2.654(1) Å (Cu), respectively. The same synthetic methodology was also applied for the preparation of a zinc derivative, $[\{(hyp)_2P_7\}_2Zn]^*Et_2O$, for which full multinuclear NMR characterization could be conducted.

Keywords: coinage metals; copper; silver; gold; main group chemistry; phosphorus; X-ray crystallography

check for updates

Citation: Roller, C.A.; Doler, B.; Fischer, R.C. Preparation and Structural Variety of Neutral Heptaphospha-Nortricyclane Derivatives of Zinc and the Coinage Metals. *Crystals* **2024**, *14*, 586. https://doi.org/10.3390/cryst14070586

Academic Editor: Elizabeth A. Hillard

Received: 29 May 2024
Revised: 11 June 2024
Accepted: 13 June 2024
Published: 26 June 2024

1. Introduction

The study of cyclic and polycyclic phosphorus compounds has been a subject of fascination for decades, with pioneering work being performed by the groups of Baudler and von Schnering, which continues to inspire further contemporary research [1,2]. After carbon, phosphorus has the strongest tendency to form homonuclear element–element bonds, with countless examples of mono- and polycyclophosphanes being reported in the literature [1–3]. Among these, the nortricyclane-type P_7 system represents an important and repeating structural motif, while the corresponding Zintl cluster, $[P_7]^{3-}$, has been studied thoroughly, in part due to its accessibility [4]. NMR spectroscopic investigations revealed a set of three signals with complex couplings at δ = −57 (apical P), −103 (bridging P^- atoms), and −162 (P atoms of a three-membered ring) ppm with measurements conducted at −60 °C [1,3,4]. Upon warming to +50 °C, convergence of the signals was observed, which could be traced back to the reversible valance tautomerism within the phosphorus backbone [1,3]. This, among other characteristics, underlines the structural parallels of the heptaphosphide anion and the organic bullvalene ($C_{10}H_{10}$) [1,3]. Structural elucidation of the $[P_7]^{3-}$ cage was conducted by von Schnering (SC-XRD analyses of Sr_3P_{14} and Ba_3P_{14}) [5,6]. Attention has also been devoted to the derivatization and functionalization of the P_7 skeleton, yielding the neutral molecular counterparts of R_3P_7. Early research in the field led to the isolation of organo-, tetrel-, and pnictogen-substituted cages [7–12]. Later, transition-metal-capped cycloheptaphosphanes were also reported [13–15]. Only recently was the Mehta group able to further show the functionalization of tetrel substituents toward heteroallenes [16]. Selected examples are given in Figure 1.

Silyl-substituted P_7-nortricyclane cages have already been studied at our institute in the past [7,8,10]. Hassler was able to show that treatment of $(tms)_3P_7$ (first isolated by Fritz in the 1970s) [17] with hyp-Cl (hyp = 'hypersilyl' = $Si(SiMe_3)_3$) leads to a silyl exchange reaction, yielding the heteroleptic derivative $(hyp)_2(tms)P_7$ [8]. Similar methodologies have also been used for the preparation of $(Ph_3Si)_3P_7$ and $(Me_3Pb)_3P_7$ from $(tms)_3P_7$ [9].

Despite these advances in the field, Hassler and coworkers were not able to achieve functionalization of the P_7 core (from $(tms)_2P_7M$ (M = Li, K)) without degradation of the backbone (i.e., in alkylation reactions with $(MeO)_2SO_2$, MeI, $BrCH_2CH_2Br$, $PhCH_2Br$, or $PhCH_2N(CH_3)_3Br$) or the formation of insoluble polymeric materials when $MgBr_2$, Ph_2SnCl_2, or $HgCl_2$ were used [8].

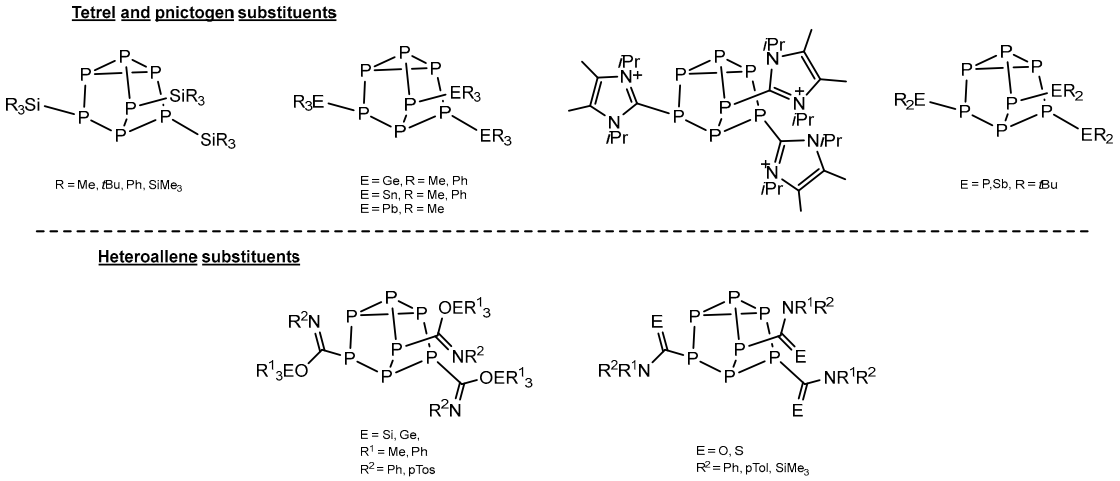

Figure 1. Selected examples of P_7 cages bearing different types of substituents.

The study of transition-metal-functionalized P_7 derivatives has thus far been dominated by anionic compounds [4]. While the η^1- and η^2- coordination modes retain the initial structure of the P_7 skeleton, higher coordination patterns (i.e., η^4) are generally accompanied by the insertion of the metal atoms into P-P bonds, causing the partial degradation or rearrangement of the heptaphosphane backbone [13,14,18–22]. Among the examples presented in the literature, only three neutral transition-metal-substituted heptaphosphane compounds are mentioned, with just one containing a group 11 metal (see Figure 2) [13–15]. Synthesis of the gold-containing derivative was conducted *via* a pathway similar to the one we used for the preparation of the herein-reported compounds **4**–**7** with $(tms)_3P_7$ as a precursor in reactions with the N-heterocyclic carbene Au(I) complex $NHC^{dipp}AuCl$. A 1:3 ratio of the corresponding starting materials afforded an uncharged trinuclear complex (accompanied by the formation of 3 eq of tms-Cl). The gold atoms in this compound show the expected linear twofold coordination geometry [14].

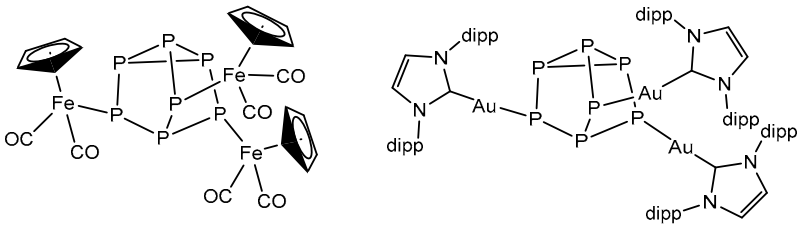

Figure 2. Neutral transition metal derivatives based on the P_7-nortricyclane cage.

2. Results and Discussion

Synthesis of precursors $(tms)_3P_7$ (**1**) and the heteroleptic nortricyclane $(hyp)_2(tms)P_7$ (**3**) was conducted following procedures described in the literature [8,17]. **1** is conveniently accessible from the Zintl anion $(Na/K)_3P_7$ and trimethylchlorosilane from a salt metathesis reaction. For the first step—the synthesis of $(Na/K)_3P_7$—a sodium–potassium alloy was prepared, and DME was added as a solvent before adding the corresponding amount of red phosphorus powder. After heating the mixture to reflux overnight and removing the solvent under reduced pressure the next day, freshly distilled tms-Cl was added at −50 °C to toluene. **1** was obtained in moderate yields after a work-up (see the Section 4).

Spectroscopic data were in accordance with values in the literature, displaying resonances at −1.5 ppm (three equatorial Me_3Si-substituted P atoms), −101.9 ppm (one apical P atom), and −159.1 ppm (basal P atoms) in $\{^1H\}^{31}P$ spectra [8,17].

Upon crystallization from toluene at −30 °, Fritz and coworkers (and Hassler in later work) obtained the chiral cage compound **1** as a racemic conglomerate of enantiopure crystals of the sym-isomers (monoclinic space group $P2_{(1)}$, no. 4, CCDC 1178312) [8,10,17]. In our hands, recrystallization of **1** from *n*-pentane led to the isolation of a new polymorph of **1** (orthorhombic space group $Pna2_{(1)}$, no. 33). As the original X-ray structure determination of **1** was carried out at room temperature, and hence shows systematically shortened bond lengths, an additional data set for the monoclinic structure was collected at 100 K. The structural parameters of the P_7 framework in **1** do not differ significantly between the two polymorphs at 100 K, with average P-P distances of 2.20 Å and an average angle of 98.3° for the apical phosphorus atom in both cases. The longest P-P distances are invariably found within the basal three-membered ring at values between 2.217(3) to 2.222(3) Å for the monoclinic structure known in the literature and 2.218(5) to 2.221(5) Å for the new orthorhombic polymorph. Additional structural parameters and refinement details for the new polymorph of $(tms)_3P_7$ are included in the Supporting Information.

Furthermore, after the isolation of a major fraction of crystalline compound **1**, the concentration of the supernatant toluene solution and storage at −35 °C yielded a small amount of bright yellow crystals of undecaphosphane $(tms)_3P_{11}$, **2**. The preparation of **2** was previously reported by von Schnering and coworkers [23], but the much higher air and moisture sensitivity of **2** in comparison to the smaller heptaphosphane $(tms)_3P_7$ has hampered SC-XRD structural analysis in the past. Hence, only unit cell parameters and a preliminary structure based on 390 reflections have been reported ibidem, but neither atomic positions nor anisotropic displacement parameters of **2** are available in the CCDC. In agreement with the previously reported unit cell parameters, **2** crystallized as the asymmetrical of the two possible isomers of a tris trimethylsilyl-substituted pentacyclo[6.3.0.$-0^{2,6}$.$0^{3,10}$.$0^{5,9}$]undecaphosphane. In **2**, the average P-P distance is 2.218 Å; the longest bonds extend from phosphorus atoms P3 and P7 with values of 2.226(2) and 2.263(2) Å, respectively (c.f. Figure 3).

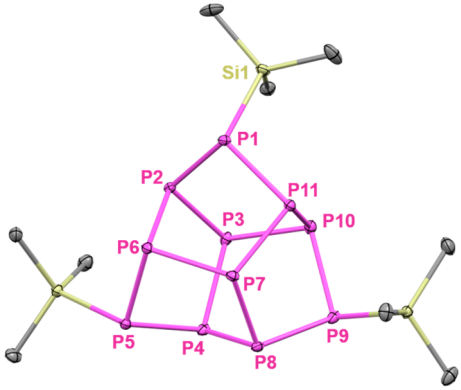

Figure 3. Molecular structure of $(tms)_3P_{11}$ (**2**). Atoms are shown as 30% shaped ellipsoids. Hydrogens are omitted for clarity. P atoms in purple, Si in pale yellow, C in grey. Selected bond lengths [Å] and angles [°] for **2** are: P1-P2 2.195(2), P1-P11 2.195(2), P2-P3 2.240(2), P2-P6 2.196(2), P3-P4 2.259(2), P3-P10 2.255(2), P4-P5 2.204(2), P4-P8 2.202(2), P5-P6 2.197(2), P7-P8 2.263(2), P7-P11 2.251(2), P8-P9 2.198(2), P9-P10 2.188(2), P10-P11 2.189(2), P1-P2-P6 101.15(7), P1-P2-P3 97.51(7), P1-P11-P10 90.72(7), P1-P11-P7 107.75(7), P2-P6-P5 99.34(7), P2-P6-P7 103.76(7), P2-P3-P4 101.04(7), P2-P3-P10 102.61(7), Si1-P1-P2 107.29(7).

For the preparation of the heteroleptic P_7 cage $(hyp)_2tmsP_7$, **3**, the silyl exchange reaction between **1** and hyp-Cl (hyp = 'hypersilyl' = $Si(SiMe_3)_3$) was performed according to Scheme 1. To avoid the formation of hyp_3P_7, which is inseparable from **3** *via* recrystallization, a DME solution of exactly two equivalents of hyp-Cl was slowly added to a

DME solution of **1**, while the temperature was maintained at −50 °C. After removal of the DME and the tms-Cl, concomitantly formed under reduced pressure, recrystallization from toluene gave $(hyp)_2(tms)P_7$ (**3**) in an 86% yield as yellow crystals. Analytical data for **3** are in accordance with literature values, showing resonances at −6.4 (1 + 2P, *P*(tms) + 2*P*(hyp)), −103.5 (1P, apical), −150.1 (1P, basal, *P*P(tms)), and −168.3 ppm (2P, basal, *P*P(hyp)) in $\{^1H\}^{31}P$ spectra [8,10]. An overview of the synthetic steps to create compounds **1**, **2,** and **3** is provided in Scheme 1.

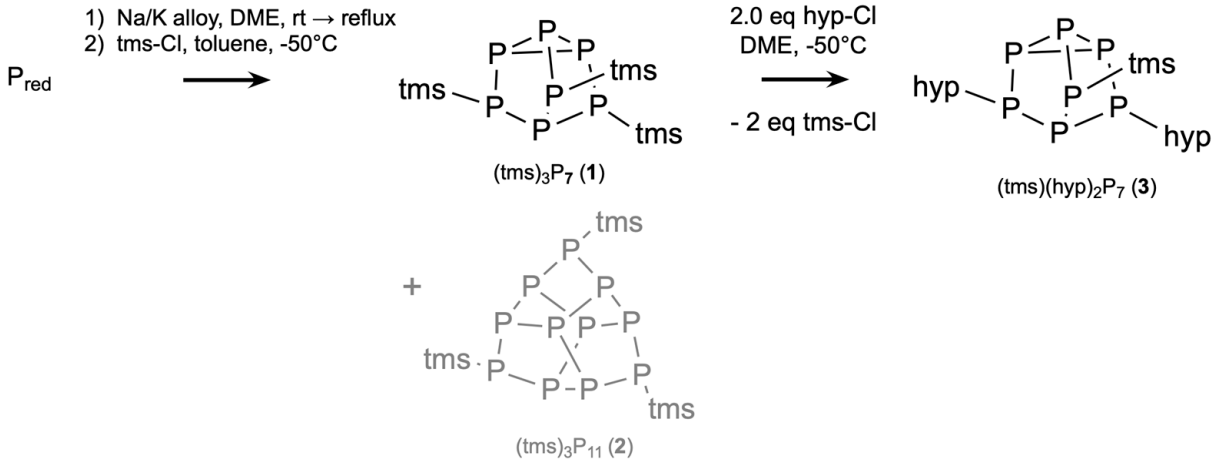

Scheme 1. Synthetic protocol used for the preparation of $(tms)_3P_7$ (**1**), side product $(tms)_3P_{11}$, (**2**), and $(hyp)_2(tms)P_7$ (**3**).

With the heterosubstituted $(hyp)_2(tms)P_7$ cage **3** at hand, and considering the steric shielding and low chemical reactivity of hypersilyl-phosphorus bonds in comparison to the less encumbered trimethyl-silyl groups, we were tempted to explore the possibility of synthesizing neutral, hitherto unknown, mono-metalated derivatives $[(hyp)_2P_7]_nM$ of heptaphosphanortricyclanes.

In an attempt to prepare uncharged group 11 derivatives stabilized by the bis(hypersilyl)-substituted fragment $(hyp)_2P_7$, we reacted $(hyp)_2(tms)P_7$, **3**, with coinage metal salts M(I)X. Hence, the addition of solutions of **3** to equimolar suspensions of MX (M = Cu, Ag, Au; X = Br, CF_3SO_3 (OTf), Cl*SMe_2) resulted in the rapid color change of the reaction mixtures, the consumption of the suspended group 11 salts and, finally, the precipitation of the targeted derivatization products. In the case of Cu, the consumption of the starting material from the reaction mixture completes after approximately 1 h, as monitored by $\{^1H\}^{31}P$ NMR spectroscopy of reaction aliquots, while the formation of the Ag derivative takes only approximately 15 min to complete at room temperature. Reactions with AuCl*SMe_2 are even faster, and the dimeric product $[(hyp)_2P_7Au]_2$ (**4**) can be isolated as a brown crystalline material after 1–2 min. The reactions towards compounds **4**–**7** are summarized in Scheme 2.

The compositions of the thus obtained coinage metal P_7 cage derivatives **4**–**6** were structurally authenticated by SC-XRD analysis. A summary of selected structural parameters for the gold (**4**), silver (**5**), and copper (**6**) derivatives is provided in Table 1.

Crystallographic investigations of the gold-containing product **4** revealed the formation of a dinuclear $[(hyp)_2P_7Au]_2$ compound (c.f. Figure 4. In the solid state, **4** exists as a dinuclear cluster, which contains a $[Au_2]^{2+}$ fragment ligated to two $[(hyp)_2P_7]^-$ -moieties in a $\mu,\eta^{1:1}$ coordination mode. Comparable heteronuclear, dianionic silver, and gold clusters $[M_2(HP_7)_2]^{2-}$ (M = Au, Ag) were isolated from reactions of MCl (M = Ag, Au) or $[M(norbornene)_3][SbF_6]$ with ethylenediamine solutions of $[P_7]^{3-}$ [4,24]. In these, and also in **4**, the the P_7 fragments adopt an "up–down" orientation with respect to each other [24]. Furthermore, the gold and silver complexes $[M_2(HP_7)_2]^{2-}$ and $[(hyp)_2P_7Au]_2$ are structurally related to the wel-known hexadecaphosphadiide $[P_{16}]^{2-}$ originally reported by Hönle and subsequently by Baudler. In this, two P_7 fragments are linked in an "up–up"

fashion *via* a diphospha bridge [25,26], hence being closely related to the structure of violet phosphorus (see Figure 5). In the case of the neutral compound **4**, we presume that, aside from packing effects, the steric demand of the encumbering hypersilyl substituents is responsible for the observed "up–down" orientation.

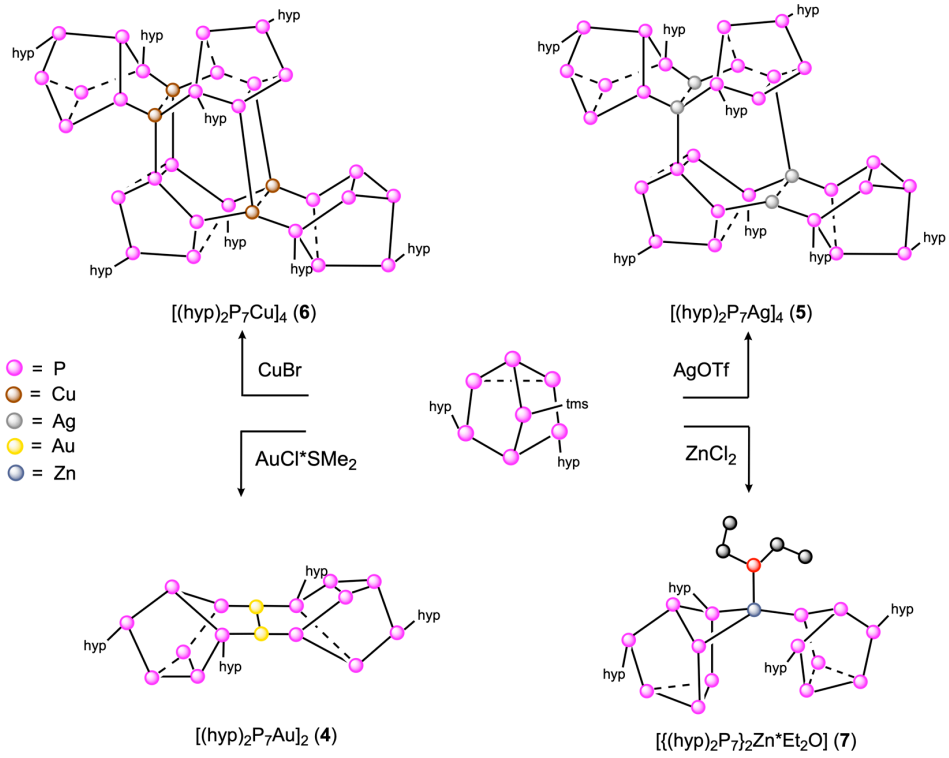

Scheme 2. Synthesis of coinage metal derivatives **4**–**6** and Zn derivative **7** from $(hyp)_2(tms)P_7$ **3**.

Table 1. Selected structural parameters (bond distances [Å] and angles [°]) of coinage metal heptaphosphide derivatives **4**, **5**, and **6** ($^{\#}$ refers to symmetry generated sites).

	4		**5**		**6**
Au1-Au1 $^{\#}$	2.9542(2)	Ag1-Ag2	2.8833(6)	Cu1-Cu2	2.654(1)
Au1-P1	2.322(1)	Ag1-P1	2.494(1)	Cu1-P1	2.287(3)
Au1-P3 $^{\#}$	2.328(1)	Ag1-P13	2.450(1)	Cu1-P13	2.524(2)
P1-P2	2.192(1)	P1-P2	2.202(2)	P1-P2	2.151(2)
P1-P5	2.199(2)	P1-P5	2.214(2)	P1-P7	2.166(2)
P1···P3	3.293(2)	P1···P7	3.295(2)	P1···P5	3.340(2)
P2-P3	2.170(2)	P2-P3	2.195(2)	P2-P3	2.218(3)
P2-P7	2.197(2)	P2-P7	2.159(2)	P2-P4	2.239(2)
P3-P4	2.197(2)	P3-P4	2.186(3)	P3-P4	2.230(3)
P4-P5	2.222(2)	P4-P5	2.228(2)	P3-P6	2.200(2)
P4-P6	2.216(2)	P4-P6	2.226(2)	P4-P5	2.225(2)
P5-P6	2.220(2)	P5-P6	2.218(2)	P5-P7	2.198(3)
P6-P7	2.201(2)	P6-P7	2.169(2)	P6-P7	2.196(3)
		Ag1-$P6_{dimer2}$	2.581(2)	Cu1-$P4_{dimer2}$	2.411(2)
				Cu2-$P2_{dimer2}$	2.252(2)
P1-Au1-P3 $^{\#}$	171.64(4)	P1-Ag1-P13	138.86(5)	P1-Cu1-P13	110.23(7)
P1-Au1-Au1 $^{\#}$	91.55(3)	P1-Ag1-Ag2	91.37(4)	P1-Cu1-Cu2	95.88(6)
P_{apex}-P1-Au1	110.96(6)	P_{apex}-P1-Ag1	110.21(7)	P_{apex}-P1-M1	105.78(9)

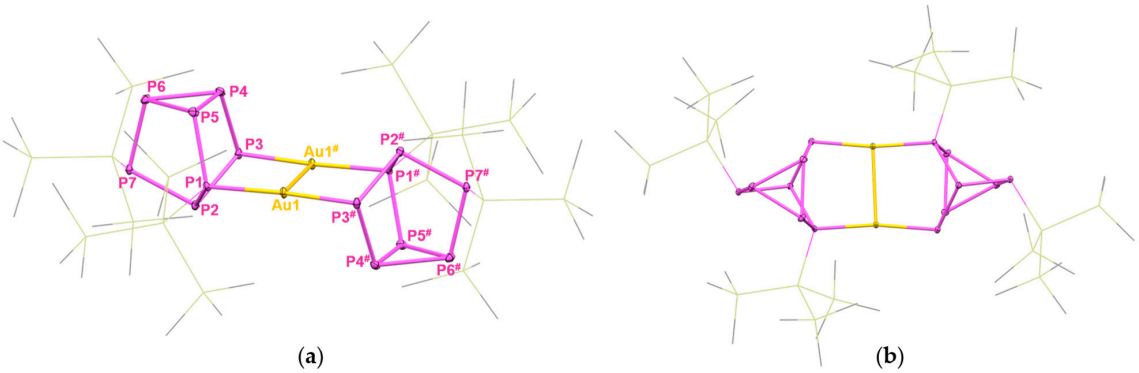

Figure 4. Molecular structure of $[(hyp)_2P_7Au]_2$ (**4**). Heavier atoms incorporated into the core structure of the cage are shown as 30% shaped ellipsoids. Hydrogens are omitted for clarity. (**a**) Side view. (**b**) Top view. (P: purple, Au: yellow, Si: pale yellow, C: grey; # refers to symmetry-generated sites).

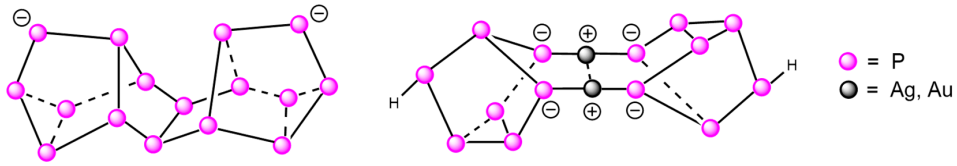

Figure 5. Structures of anionic compounds $[P_{16}]^{2-}$ (left) and $[M_2(HP_7)_2]^{2-}$ (M = Ag, Au; right) related to $[(hyp)_2P_7Au]_2$.

4 shows a planar, T-shaped coordination geometry around both Au atoms. The interatomic Au–Au distance of 2.9542(2) Å is somewhat shorter in comparison to Goicoechea's anionic species (3.047(1) Å) and the majority of compounds with three-coordinate Au atoms and direct Au–Au contacts, as reported in the Cambridge Crystallographic Database (average ca. 3.04 Å) [24]. This points towards a closed-shell aurophilic interaction of the gold atoms in **4**. The term "aurophilic" was first introduced by Schmidbaur and coworkers and is generally recognized as dispersion forces of energies around 29–46 kJ/mol and is hence similar to the values involved in hydrogen bonding [27–32].

In contrast to the largely identical structures of the previously reported silver and gold compounds $[M_2(HP_7)_2]^{2-}$ (M = Au, Ag), the SC-XRD structure analysis of the silver-containing derivative **5** revealed a different structure to **4**. In contrast to the dimeric product **4**, the silver derivative $[(hyp)_2P_7Ag]_4$ **5** exhibits a tetrameric arrangement in the solid state in which two $[(hyp)_2P_7Ag]_2$ fragments are linked over a crystallographic inversion center *via* additional Ag–P interactions (c.f. Figure 6).

Each of the two dimeric fragments $[(hyp)_2P_7Ag]_2$ in **5** yet again feature a bimetallic core coordinated in a $\mu,\eta^{1:1}$ coordination pattern. However, in contrast to gold derivative **4**, **5** is bent along the two bridging silver atoms, resembling the "up–up" configuration found in the previously mentioned polyphosphide $[P_{16}]^{2-}$ [24,25]. The inverted geometry of the P_7 units in **5**, as compared to **4**, is likely a result of the coordination towards a second $[Ag(hyp_2P_7)]_2$-fragment to form the final tetrameric structure in which the crystallographic inversion center is located at the center of gravity. The rather unsymmetrical, tetrameric arrangement in **5** features a short donor–acceptor bond of 2.582(1) Å between one of the silver atoms (Ag1) with one of the phosphorus atoms ($P6^{\#}$) of the basal, three-membered ring system of the symmetry-generated (third) heptaphosphide cage, while the Ag2 is located at a distance of 3.131(2) Å from $P5^{\#}$. The respective P–Ag–P angles are 133.86(5)° (P7-Ag2-P12) and 138.86(5)° (P1-Ag1-P13). The Ag1–Ag2 internuclear distance in **5** is 2.8833(6) Å, and is hence again slightly shortened in comparison to Goicoechea's anionic complex $[Ag_2(HP_7)_2]^{2-}$ (2.947(1) Å) [24,33]. Once more, this suggests a closed-shell, argentophilic, interaction between two d^{10} metal centers [24,33–36].

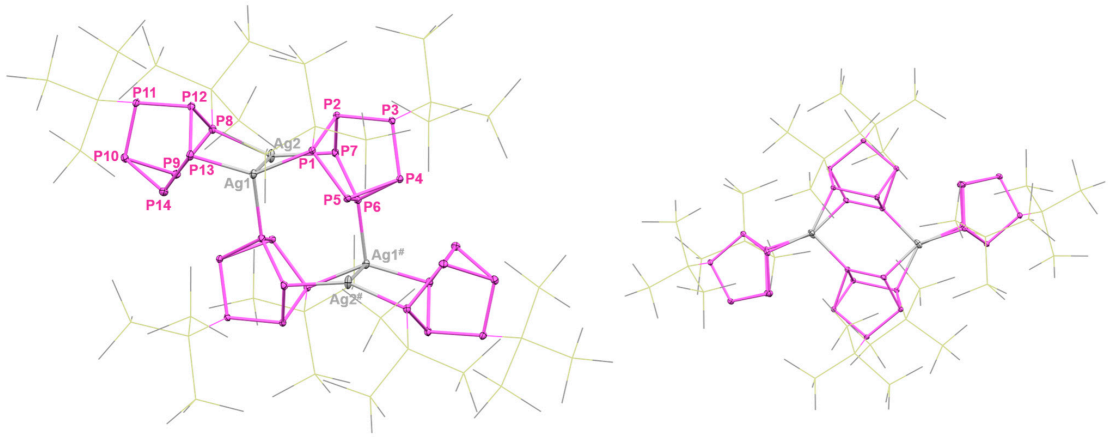

(**a**) (**b**)

Figure 6. Molecular structure of $[(hyp)_2P_7Ag]_4$ (**5**). Heavier atoms incorporated into the core structure of the cage are shown as 30% shaped ellipsoids. Hydrogens are omitted for clarity. (**a**) Side view. (**b**) Top view. (P: purple, Ag: light grey, Si: pale yellow, C: grey; # refers to symmetry-generated sites).

The reaction of the heteroleptic P_7-notricyclane cage **3** with CuBr yielded the polycyclic copper derivative **6**. **6**, like the aforementioned **5**, exhibits a tetrameric arrangement in the solid state (c.f. Figure 7). In contrast to **5**, the cluster of the copper derivative **6** features an almost perfectly symmetrical hexagonal–prismatic structure around the inversion center with Cu–P distances of 2.247(2)–2.556(2) Å and a short Cu1–Cu2 separation of 2.654(1) Å. The P–P bonds in the hexagonal prismatic core are short at 2.151(2)–2.239(1) Å while the Cu–Cu–P angles are around 90° with values between 79.77(8) and 101.13(8)°.

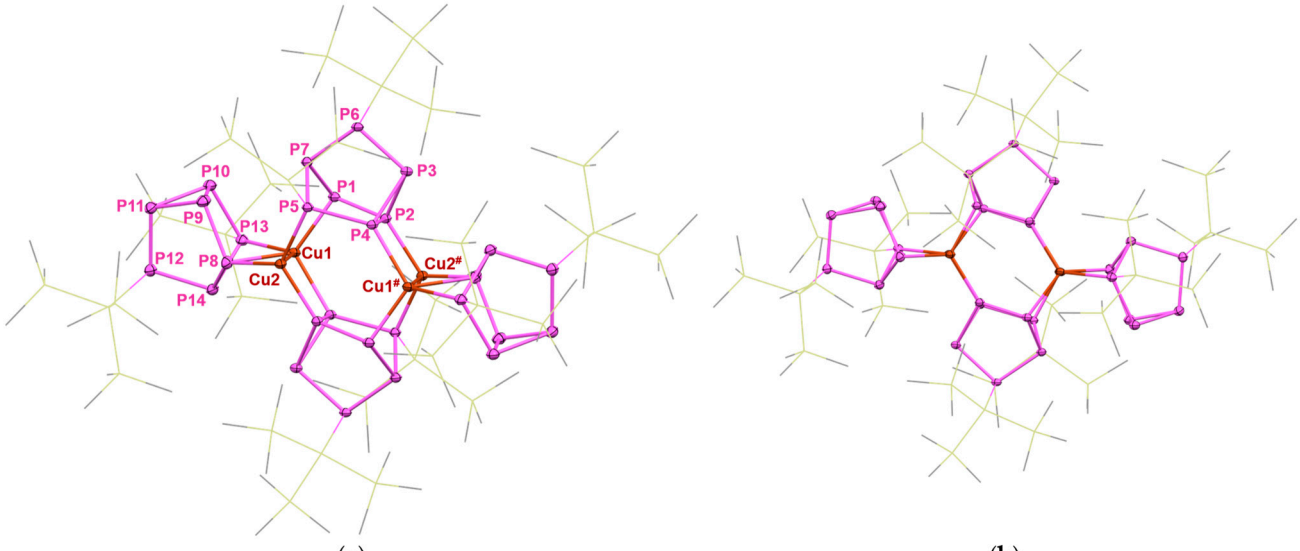

(**a**) (**b**)

Figure 7. Molecular structure of $[(hyp)_2P_7Cu]_4$ (**6**). Heavier atoms incorporated into the core structure of the cage are shown as 30% shaped ellipsoids. Hydrogens are omitted for clarity. (**a**) Side view. (**b**) Top view. (P: purple, Cu: brown, Si: pale yellow, C: grey; # refers to symmetry-generated sites).

In addition to the d^{10} coinage metal ions Au^+, Ag^+, and Cu^+, we investigated the coordination behavior of the $[(hyp)_2P_7]^-$-fragment towards the dicationic d^{10} Zn^{2+}-ion. The colorless, neutral, mononuclear zinc complex **7**, $[\{(hyp)_2P_7\}_2Zn]$ was isolated from the reaction of **3** with $ZnCl_2$ in diethyl ether in very good yields (c.f. Supporting Information). **7** crystallizes in the monoclinic space group $C2_{/c}$ (no. 15). Single crystal X-ray structure analysis revealed the "up–up" isomer with the central zinc atom being disordered over

two positions (50:50 occupancy) in close proximity to the crystallographic two-fold axis (c.f. Figure 8).

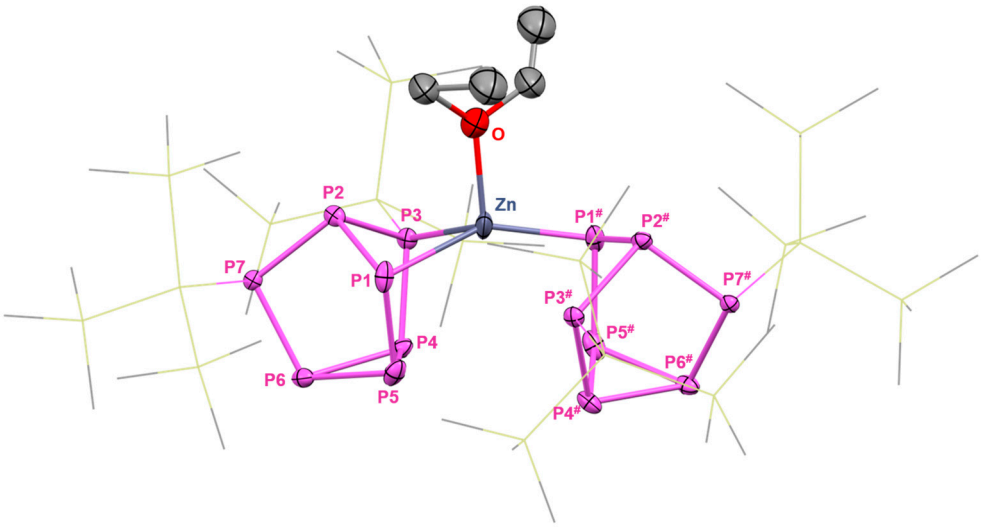

Figure 8. Molecular structure of [{(hyp)$_2$P$_7$}$_2$Zn*Et$_2$O] (**7**). Heavier atoms incorporated into the core structure of the cage, as well as donating molecules, are shown as 30% shaped ellipsoids. Hydrogens are omitted for clarity. (P: purple, Zn: blue-grey, Si: pale yellow, O: red, C: grey; # refers to symmetry-generated sites).

The zinc atom is engaged in a slightly distorted tetrahedral coordination geometry towards three phosphorus atoms and the oxygen of a coordinated solvent molecule diethyl ether with Zn–P distances between 2.259(1) and 2.589(1) Å and a Zn–O separation of 2.108(7) Å. Similar to the skeletal parameters of the P$_7$ framework in **4**–**6**, P–P bonds connecting the Zn-coordinated phosphorus atoms P1 and P3 to the rest of the P7 structure are short with values below 2.20 Å ranging from 2.163(1) to 2.183(1) Å. Additional structural parameters for **7** are provided in Table 2.

Table 2. Selected structural parameters (bond distances [Å] and angles [°]) of the zinc-derivatized heptaphosphide compound **7**. (# refers to symmetry generated sites).

	7
Zn-P1	2.434(1)
Zn-P3	2.5839(9)
Zn-P1$^{\#}$	2.259(1)
Zn···P3 $^{\#}$	3.4284(9)
Zn-O	2.108(7)
P1-P2	2.1627(9)
P1-P5	2.175(1)
P1···P3	3.1913(8)
P2-P3	2.1713(9)
P2-P7	2.162(1)
P3-P4	2.183(1)
P4-P5	2.2283(9)
P4-P6	2.211(1)
P5-P6	2.215(1)
P6-P7	2.179(1)
P1-Zn-P3	78.93(3)
P1-Zn-P1 $^{\#}$	145.54(5)
P1-Zn-P3 $^{\#}$	85.80(3)
P3-Zn-P3 $^{\#}$	142.31(3)
P1-Zn-O	103.1(2)

NMR Spectroscopy of **4** *and* **7**

Despite compounds **4**–**6** being uncharged and prepared from toluene reaction mixtures, the silver and copper complexes proved completely insoluble in organic solvents including aromatic (benzene, toluene), ethereal (THF, DME, diethylether), and chlorinated (CH_2Cl_2 and $CHCl_3$) solvents. However, the gold complex **4** proved to be very sparingly soluble in THF-d_8 with $\{^1H\}^{31}P$ resonances at 57.5 (2 P atoms), −28.2, −107.7, −143.2, −184.4, and −192.1 ppms (one P atom each). Nevertheless, the zinc derivative **7** was originally obtained *via* crystallization from diethyl ether but is sufficiently soluble in benzene for a full heteronuclear NMR spectroscopic characterization. The proton-decoupled ^{31}P NMR spectrum shows the expected (1/1/1): 1:1:1:1 signal intensity ratio with chemical shifts centered from around 13.2 to −198.7 ppm as shown in Figure 9. In comparison, for starting material **3,** the resonance of the apical phosphorus atom (−84.4 ppm in **7**) is shifted downfield by some 19 ppm while the resonances for the basal P atoms are observed at −117.7, −154.6, and −198.7 ppm, respectively. The anionic atom and both hypersilylated P atoms are downfield shifted and resonate between +28 and +1 ppm. This behavior is in agreement with a largely localized negative charge and hences with the anionic character of the metalated phosphorus atom.

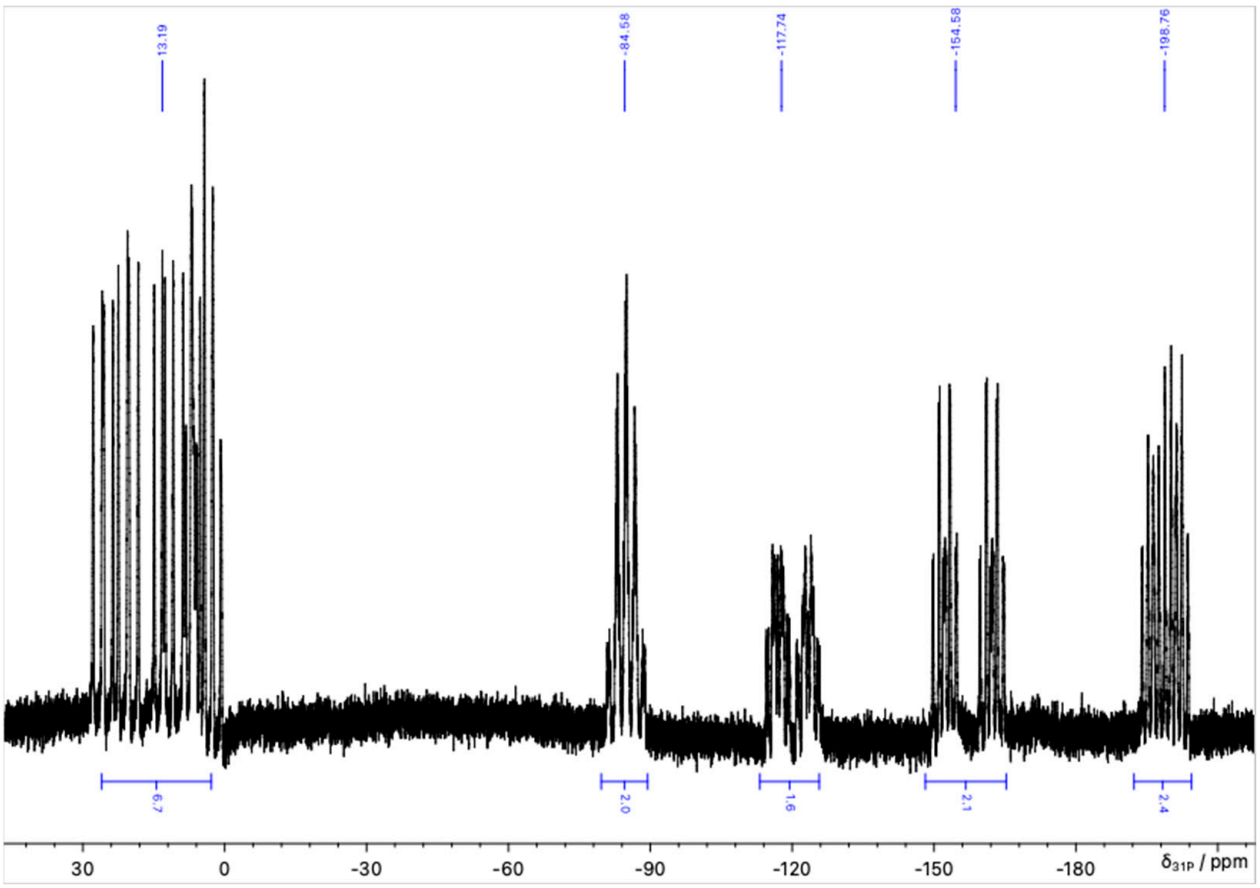

Figure 9. $\{^1H\}^{31}P$ NMR spectrum of **7**.

3. Conclusions

Starting from the heterosubstituted heptaphospha-nortricyclane cage compounds $(hyp)_2(tms)P_7$ **3**, the respective neutral Au(I), Ag(I), and Cu(I) derivatives $[(hyp)_2P_7M]_n$ (M = Au, n = 2; M = Ag, Cu, n = 4) have been prepared *via* halodesilylation reactions under cleavage of the sterically less shielded trimethyl silyl group. All three coinage metal derivatives **4**–**6** feature short metal–metal distances that amount to 2.9542(2) Å (Au), 2.8833(6) Å (Ag), and 2.654(1) Å (Cu), respectively. Moreover, the same methodology allowed for the

preparation of a zinc derivative [{$(hyp)_2P_7$}$_2$Zn]*Et_2O. Preliminary experiments with other metal halides and pseudohalides MX_n suggest the possibility of extending the synthetic strategy towards the preparation of other neutral, $(hyp)_2P_7$-supported metal complexes.

4. Experimental Section

4.1. Materials and Methods

All manipulations, including compounds showing sensitivity towards air or moisture, were performed under an inert atmosphere using standard Schlenk tube techniques or in a nitrogen flushed glovebox, UNILAB (M. Braun Inertgassystems GmbH, Garching, Germany). Dried and deoxygenated solvents were obtained from a solvent drying system PureSolve MD5 (Innovative Technology Inc., Amesbury, MA, USA). C_6D_6 and THF-d_8 for NMR measurements were degassed using the 'freeze–pump–thaw' method and stored over 3 Å molecular sieves. All Raman measurements were performed in a capillary using a Raman Station 400F (Perkin Elmer, Waltham, MA, USA) with a built-in 350 mW laser operating at 785 nm.

4.1.1. NMR-Spectroscopy

^{1}H (400.13 MHz), ^{13}C (100.613 MHz), ^{29}Si (79.50 MHz), and ^{31}P (161.976 MHz) NMR spectra, as well as all 2D experiments, were recorded on a QUAD ONE 400 MHz NMR spectrometer (QUAD Systems Ltd., Dietlikon, Switzerland) at 25 °C. Spectra were referenced to solvent residual signals, where applicable. Chemical shifts are given in ppm relative to TMS regarding ^{1}H, ^{13}C, and ^{29}Si. ^{31}P chemical shifts are given relative to 80% H_3PO_4. Coupling constants (^nJ) are reported in Hertz (Hz).

4.1.2. Single Crystal X-ray Diffraction

For single-crystal X-ray diffractometry, suitable crystals were selected and covered with a layer of silicone oil. A single crystal was picked and subsequently mounted on a glass rod on a copper pin, and was placed in a cold N_2 stream (T = 100 K, Oxford 700 Cryometer, Oxford Cryosystems, Oxford, UK). XRD data collection was performed on a Bruker APEX II diffractometer (Bruker AXS Advanced Xray Solutions GmbH, Karlsruhe, Germany) with use of Mo Kα radiation (λ = 0.71073 Å) from an IμS microsource and an APEX II CCD area detector. For empirical absorption corrections, SADABS was used [37,38]. Structures were solved using either direct methods or the Patterson option in SHELXS. Refinement of obtained structures was performed utilizing SHELXL [39,40]. CIF files were edited, validated, and formatted with the program OLEX2 [41]. The assignment of space groups and structural solutions were validated using PLATON [42,43]. All non-hydrogen atoms were refined anisotropically. All hydrogen atoms were placed in calculated positions according to standard bond lengths and angles using riding models. Details about measurements and crystallographic data are provided in the Supporting Information for this article.

4.2. Syntheses

4.2.1. Synthesis of 3,5,7-Tris(trimethylsilyl)tricyclo[2.2.1.02,6]heptaphosphane ($(tms)_3P_7$, **1**)

1 was prepared following adapted procedures from the literature [8,10,17]. First, 3.54 g potassium (90.5 mmol, 1.6 eq), and 2.98 g sodium (130 mmol, 2.3 eq) were transferred into a nitrogen-filled 500 mL three-necked round bottom flask equipped with a reflux condenser and a dropping funnel and were subsequently melted by carefully heating to form a liquid alloy. To this alloy, 200 mL of dry DME was added and the solvent was heated to reflux for 30 min, which resulted in the dark blue color of the organic phase. After the reaction solution was allowed to cool to room temperature, 11.32 g red phosphorus powder (366 mmol, 6.4 eq) was cautiously added to the mixture. The reaction solution briefly acquired a characteristic red color and was afterwards heated to reflux overnight. On the next day, the reaction was cooled to room temperature. A black precipitate in a

yellow-green solution was obtained. Subsequently, the solvent was removed under reduced pressure, yielding $(Na/K)_3P_7$ as a dark red solid.

For the next step, $(Na/K)_3P_7$ was dispersed in 300 mL of dry toluene and cooled to −50 °C. Over a period of 30 min, 30 mL of freshly distilled chlorotrimethylsilane (236 mmol, 4.1 eq) was added dropwise with a dropping funnel. Temperatures around −50 °C were retained for ca. 3 h, after which the reaction mixture was allowed to warm to room temperature overnight to yield a greyish precipitate together with a bright yellow organic phase. The mixture was filtered and the grey precipitate was washed twice with 75 mL of dry hexanes. The solvent of the yellow filtrate was removed under reduced pressure to incipient crystallization. Cooling to −30 °C over night yielded **1** as a yellow crystalline material. Analytical data for **1** are in accordance with literature values [8,10,17].

Yield: 15.09 g (60%), yellow solid. Anal. Calcd. For $C_9H_{27}Si_3P_7$: C, 24.77; H, 6.24. Found: C, 24.49; H, 6.37.

^{31}P NMR (161.976 MHz, THF-d_8) δ −1.5 (m, 3 P), −101.9 (m, 1 P), −159.1 (m, 3 P) ppm.

The concentration of the supernatant and storage at −35 °C yielded a crop of bright yellow, very air- and moisture-sensitive crystals of **2**, which were suitable for SC-XRD structure analysis. Analytical data for **2** are in accordance with literature values [23].

4.2.2. Synthesis of 3,5-Bis(1,1,1,3,3,3-hexamethyl-2-(trimethylsilyl)trisilan-2-yl)-7-(trimethylsilyl)tricyclo[2.2.1.02,6]heptaphosphane ((hyp)$_2$(tms)P$_7$, **3**)

3 was prepared following an adapted procedure from the literature [8]. In a dry 500 mL three-necked round bottom flask equipped with a dropping funnel, 2.00 g $(tms)_3P_7$ (**1**, 4.58 mmol, 1.0 eq) was dissolved in 300 mL of dry DME and cooled to −50 °C. Then, 2.60 g hypersilyl chloride (9.18 mmol, 2.0 eq) was dissolved in 100 mL dry DME, transferred into the dropping funnel, and slowly added to the reaction solution, which resulted in the formation of a light yellow suspension. Temperatures of around −50 °C were held over 2 h before the reaction mixture was allowed to slowly warm to room temperature overnight. The solvent was removed under reduced pressure, and the resulting yellow solid was taken up in 50 mL toluene and extracted through a filter tipped capillary to remove insoluble polyphosphanes. The solvent was removed under reduced pressure to give $(hyp)_2(tms)P_7$ (**3**) as a yellow solid. Analytical data for **3** are in accordance with literature values [8].

Yield: 3.10 g (86%), yellow solid. Anal. Calcd. For $C_{21}H_{63}Si_9P_7$: C, 32.12; H, 8.09. Found: C, 31.69; H, 7.78.

^{31}P NMR (161.976 MHz, THF-d_8) δ 1.0 (t, 1 P), −6.4 (t, 1 P), −13.4 (t, 1 P), −104.2 (m, 1 P), −150.9 (m, 1 P), −169.1 (m, 2 P) ppm. Raman (140 mW) 102, 172, 220, 271, 330, 357, 389, 443, 503, 630, 691, 747, 2890, 2949.

4.2.3. Synthesis of $[hyp_2P_7Au]_2$ (**4**)

A clear yellow solution of 128 mg $(hyp)_2(tms)P_7$ (**3**, 0.17 mmol, 1.0 eq) in 4 ml of dry toluene was added to a suspension of 50.0 mg AuCl*SMe_2 (0.17 mmol, 1.0 eq) and 44.5 mg Ph_3P (0.17 mmol, 1.0 eq) in 3 ml of dry toluene. The reaction mixture briefly turned dark brown and a brown precipitate of **4** formed after 1–2 min. Filtration and washing with toluene (two times, ca. 3 ml) resulted in **4** in the form of pale brown crystals.

Yield: 275 mg (73%), brown crystalline solid. ^{31}P NMR (161.976 MHz, THF-d_8) δ 57.5 (m, 2 P), −28.2 (m, 1 P), −107.7 (m, 1 P), −143.2 (m, 1 P), −184.4 (m, 1 P) and −192.1 (m, 1 P).

Raman (140 mW) 101, 176, 263, 406, 522, 555, 627, 678, 999, 1029, 1093, 2912.

4.2.4. Synthesis of $[hyp_2P_7Ag]_4$ (**5**)

A solution of 106 mg $(hyp)_2(tms)P_7$ (**3**, 0.13 mmol, 1.0 eq) in 4 ml of dry toluene was added to a suspension of 33.9 mg $AgCF_3SO_3$ (0.13 mmol, 1.0 eq) and 24.6 mg Ph_3P (0.13 mmol, 1.0 eq) in 3 ml of dry toluene. Upon addition, the solution instantly turned dark brown and, after ca. 15 min, a light brown precipitate formed. The precipitate was isolated and washed twice with 3 ml portions of toluene.

Yield: 181 mg (91%), yellow crystalline solid. Anal. Calcd. For $C_{144}H_{434}Si_{64}P_{56}Ag_4$: C, 28.21; H, 7.14. Found: C, 29.98; H, 6.94.

Raman (140 mW) 100, 171, 222, 279, 330, 400, 433, 497, 628, 687, 744, 837, 1003, 1029, 1241, 1402, 1522, 1584, 2891, 2950.

4.2.5. Synthesis of $[hyp_2P_7Cu]_4$ (**6**)

At room temperature, a solution of 105 mg $(hyp)_2(tms)P_7$ (**3**, 0.13 mmol, 1.0 eq) in 5 ml of dry THF was added to a suspension of 20.8 mg CuBr (0.15 mmol, 1.1 eq) in 5 ml of dry THF. Upon addition, the solution turned dark brown. After 1 h, the formation of a pale yellow precipitate was observed; it was isolated and washed twice with 3 ml portions of toluene.

Yield: 194 mg (87%), yellow crystalline solid. Anal. Calcd. For $C_{144}H_{434}Si_{64}P_{56}Cu_4$: C, 29.05; H, 7.35. Found: C, 28.61; H, 7.42.

Raman (140 mW) 95, 172, 235, 331, 400, 443, 471, 497, 631, 689, 745, 836, 1240, 1404, 1440, 1657, 2781, 2891, 2951.

4.2.6. Synthesis of $[\{(hyp)_2P_7\}_2Zn]\cdot OEt_2$ (**7**)

A solution of 102 mg $(hyp)_2(tms)P_7$ (**3**, 0.13 mmol, 1.0 eq) in 5 ml of Et_2O was added to a suspension of 95.4 mg $ZnCl_2$ (0.7 mmol, 0.5 eq) in 10 ml Et_2O. From the pale yellow reaction mixture, **7** precipitated as pale yellow crystals after 2 days; it was isolated *via* filtration and dried in vacuo.

Yield: 712 mg (65%), pale yellow crystals.

^{1}H NMR (400.130 MHz, C_6D_6) δ 0.41 (dd, 108 H, 72x CH_3) ppm. ^{13}C NMR (100.613 MHz, C_6D_6) δ 3.15, 3.03, 2.58 ppm. ^{29}Si HMBC NMR (79.495 MHz, C_6D_6) δ −8.7, −85.0, −86.0, −92.9 ppm. ^{31}P NMR (161.976 MHz, C_6D_6) δ 13.2 (m, 6 P), −84.4 (m, 2 P), −117.8 (m, 2 P), −154.6 (m, 2 P), −198.7 (m, 2 P) ppm. Raman (140 mW) 109, 160, 170, 224, 286, 329, 399, 432, 496, 632, 688, 750, 836, 1242, 1262, 1403, 1444, 2890, 2951.

Supplementary Materials: The following supporting information can be downloaded at: https://www.mdpi.com/article/10.3390/cryst14070586/s1, Figure S1: 31P decoupled NMR spectrum of (tms)3P7 (**1**) in THF-d8; Figure S2: 31P decoupled NMR spectrum of (hyp)2(tms)P7 (3) in THF-d8; Figure S3: 1H NMR spectrum of [(hyp)2P7]2Zn (**7**) in C6D6; Figure S4: 13C NMR spectrum of [(hyp)2P7]2Zn (**7**) in C6D6; Figure S5: 29Si INEPT NMR spectrum of [(hyp)2P7]2Zn (**7**) in C6D6; Figure S6: 31P{1H} NMR spectrum of [(hyp)2P7]2Zn (**7**) in C6D6; Figure S7: 31P{1H} NMR spectrum of [(hyp)2P7Au]2 (**4**) in THF-d8; Figure S8: Raman spectrum of (hyp)2(tms)P7 (**3**); Figure S9: Raman spectrum of (hyp)2(tms)P7 (**3**); Figure S10: Raman spectrum of [(hyp)2P7Ag]4 (**5**); Figure S11: Raman spectrum of [(hyp)2P7Cu]4 (**6**). Figure S12: Raman spectrum of [{(hyp)2P7}2Zn*Et2O] (**7**); Figure S13: Molecular structure of the novel polymorph of (tms)3P7 (**1**); Table S1: Crystal data and structure refinement of compounds **1** and **2**. Table S2: Crystal data and structure refinement of compounds **4** and **5**; Table S3: Crystal data and structure refinement of compounds **6** and **7**.

Author Contributions: Conceptualization, R.C.F.; investigation, C.A.R., B.D. and R.C.F.; writing—original draft preparation, C.A.R.; writing—review and editing, C.A.R. and R.C.F.; visualization, C.A.R.; supervision, R.C.F. All authors have read and agreed to the published version of the manuscript.

Funding: This research received no external funding.

Data Availability Statement: The spectroscopic data and tabulated crystallographic data presented in this study are included in the Supplementary Material, which can be accessed online. Deposition numbers 2353797 (**1**), 2353798 (**2**), 2353799 (**4**), 2353800 (**5**), 2353801 (**6**), and 2353802 (**7**) contain the supplementary crystallographic data for this article. The data are provided free of charge by the joint Cambridge Crystallographic Data Centre and Fachinformationszentrum Karlsruhe Access Structures service (www.ccdc.cam.ac.uk/structures (accessed on 10 June 2024)).

Acknowledgments: We gratefully acknowledge Glen J. Smales for meticulous proofreading and thorough cross-checking of this article, which greatly enhanced the report's clarity. We gratefully acknowledge the joint NAWI Graz project, a comprehensive cooperation between the University of Graz and Graz University of Technology in the natural sciences.

Conflicts of Interest: The authors declare no conflicts of interest.

References

1. Baudler, M.; Glinka, K. Monocyclic and Polycyclic Phosphanes. *Chem. Rev.* **1993**, *93*, 1623–1667. [CrossRef]
2. Von Schnering, H.-G.; Honle, W. Bridging Chasms with Polyphosphides. *Chem. Rev.* **1988**, *88*, 243–273. [CrossRef]
3. Baudler, M. Chain and Ring Phosphorus Compounds—Analogies between Phosphorus and Carbon Chemistry. *Angew. Chem. Int. Ed. Engl.* **1982**, *21*, 492–512. [CrossRef]
4. Turbervill, R.S.P.; Goicoechea, J.M. From Clusters to Unorthodox Pnictogen Sources: Solution-Phase Reactivity of $[E_7]^{3-}$ (E = P-Sb) Anions. *Chem. Rev.* **2014**, *114*, 10807–10828. [CrossRef] [PubMed]
5. Dahlmann, W.; von Schnering, H.G. Sr3P14, Ein Phosphid Mit Isolierten $P_7^{(3-)}$Gruppen. *Naturwissenschaften* **1972**, *59*, 420. [CrossRef]
6. Dahlmann, W.; von Schnering, H.G. Die Polyphosphide SrP3 Und Ba3P14. *Naturwissenschaften* **1973**, *60*, 429. [CrossRef]
7. Siegl, H.; Krumlacher, W.; Hassler, K. Synthesis and Structure of $P_7[Si(SiMe_3)_3]_3$ (Tri(Hypersilyl)Heptaphosphanortricyclane). *Monatshefte Fuer Chem.* **1999**, *130*, 139–145.
8. Noblet, P.; Dransfeld, A.; Fischer, R.; Flock, M.; Hassler, K. Derivatization of Tris(Trimethylsilyl)Heptaphosphane. *J. Organomet. Chem.* **2011**, *696*, 652–660. [CrossRef]
9. Weber, D.; Mujica, C.; von Schnering, H.G. Tris-(Trimethyl-plumbyl)-heptaphospha-nortricyclen $P_7(PbMe_3)_3$. *Angew. Chem. Int. Ed. Engl.* **1982**, *21*, 1801–1812. [CrossRef]
10. Noblet, P.; Cappello, V.; Tekautz, G.; Baumgartner, J.; Hassler, K. Heptaphosphanortricyclenes with Oligosilyl Substituents: Syntheses and Reactions. *Eur. J. Inorg. Chem.* **2011**, *2011*, 101–109. [CrossRef]
11. Fritz, G.; Schneider, H.W. Zur Synthese Der Heptaphospha-nortricyclane R_3P_7R = Et, i-Pr, n-Bu, i-Bu, SiH_2Me, SiH_3, Et_2P–$SiMe_2$. *Z. Anorg. Allg. Chem.* **1990**, *584*, 12–20. [CrossRef]
12. Fritz, G.; Layher, E.; Goesmann, H.; Hanke, D.; Persau, C. $[t\text{-}Bu_2P]_3P_7$ Und $(t\text{-}Bu_2Sb)_3P_7$ Sowie Untersuchungen Zur Bildung von Heptaphosphanen(3) Mit PMe_2-, PF_2- Und $P(CF_3)_2$-Gruppen. *Z. Allg. Anorg. Chem.* **1991**, *594*, 36–46. [CrossRef]
13. Ahlrichs, R.; Fenske, D.; Fromm, K.; Krautscheid, H.; Krautscheid, U.; Treutler, O. Zintl Anions as Starting Compounds for the Synthesis of Polynuclear Transition Metal Complexes. *Chem. Eur. J.* **1996**, *2*, 238–244. [CrossRef]
14. Jo, M.; Li, J.; Dragulescu-Andrasi, A.; Rogachev, A.Y.; Shatruk, M. Incorporation of Coinage Metal-NHC Complexes into Heptaphosphide Clusters. *Dalton Trans.* **2020**, *49*, 12955–12959. [CrossRef] [PubMed]
15. Hönle, W.; von Schnering, H.G.; Fritz, G.; Schneider, H.W. Komplexchemie P-reicher Phosphane und Silylphosphane. II. Kristall- und Molekülstrukturen von Chromcarbonylkomplexen Mit Heptaphospha-nortricyclan Als Liganden. *Z. Allg. Anorg. Chem.* **1990**, *584*, 51–70. [CrossRef]
16. Van IJzendoorn, B.; Vitorica-Yrezabal, I.J.; Whitehead, G.F.S.; Mehta, M. Heteroallene Capture and Exchange at Functionalised Heptaphosphane Clusters. *Chem. Eur. J.* **2022**, *28*, e202103737. [CrossRef] [PubMed]
17. Fritz, G.; Hoelderich, W. Ein Neuer Typ Silylphosphane; $(Me_3Si)_3P_7$, $(Me_3Si)_4P_{14}$, $(Me{=}CH_3)$. *Naturwissenschaften* **1975**, *62*, 573–575. [CrossRef]
18. Knapp, C.M.; Large, J.S.; Rees, N.H.; Goicoechea, J.M. The Bis(Hydrogenheptaphosphide)Iron(Ii) Dianion: A Zintl Ion Analogue of Ferrocene? *Chem. Commun.* **2011**, *47*, 4111–4113. [CrossRef] [PubMed]
19. Muldoon, M.J. Modern Multiphase Catalysis: New Developments in the Separation of Homogeneous Catalysts. *Dalton Trans.* **2010**, *39*, 337–348. [CrossRef]
20. Scott, C.; Eichhorn, B.W.; Rheingold, A.L.; Bott, S.G. Synthesis, Structure, and Properties of the $[E_7M(CO)_3]^{3-}$ Complexes Where E = P, As, Sb and M = Cr, Mo, W. *J. Am. Chem. Soc.* **1994**, *116*, 8077–8086.
21. Charles, S.; Fettinger, J.C.; Eichhorn, B.W. Synthesis, Structure, and Reactivities of $[\eta^2\text{-}P_7M(CO)_4]^{3-}$, $[\eta^2\text{-}HP_7M(CO)_4]^{2-}$, and $[\eta^2\text{-}RP_7M(CO)_4]^{2-}$ Zintl Ion Complexes Where M=Mo, W. *Inorg. Chem.* **1996**, *35*, 1540–1548. [CrossRef]
22. Charles, S.; Fettinger, J.C.; Bott, S.G.; Eichhorn, B.W. Synthesis and Characterization of $[\eta^4\text{-}P_7Ni(CO)]^{3-}$, $[\eta^4\text{-}HP_7Ni(CO)]^{2-}$, and $[\eta^2\text{-}P_7PtH(PPh_3)]^{2-}$: Two Electronically Equivalent Protonated Zintl Ion Complexes with Markedly Different Structures. *Chem. Commun.* **1989**, *28*, 5837. [CrossRef]
23. Von Schnering, H.G.; Fenske, D.; Hönle, W.; Binnewies, M.; Peters, K. Novel Polycyclic Phosphanes and Arsanes: $Pi_{11}(SiMe_3)_3$ and $As_7(SiMe_3)_3$. *Angew. Chem. Int. Ed. Engl.* **1979**, *18*, 679. [CrossRef]
24. Knapp, C.M.; Jackson, C.S.; Large, J.S.; Thompson, A.L.; Goicoechea, J.M. Heteroatomic Molecular Clusters Derived from Group 15 Zintl Ion Cages: Synthesis and Isolation of $[M_2(HP_7)_2]^{2-}$ (M = Ag, Au), Two Novel Cluster Anions Exhibiting Metallophilic Interactions. *Inorg. Chem.* **2011**, *50*, 4021–4028. [CrossRef]
25. Von Schnering, H.G.; Manriquez, V.; Hönle, W. Bis(Tetraphenylphosphonium) Hexadecaphosphide, a Salt Containing the Novel Polycyclic Anion $P^{2-}{}_{16}$. *Angew. Chem. Int. Ed. Engl.* **1981**, *20*, 594–595. [CrossRef]
26. Baudler, M.; Düster, D. Beiträge Zur Chemie Des Phosphors, 175 Dinatrium-Hexadecaphosphid: Darstellung Durch Spaltung von Weißem Phosphor Mit Natrium. *Z. Naturforsch.* **1987**, *42*, 335–336. [CrossRef]
27. Schmidbaur, H.; Scherbaum, F.; Huber, B.; Müller, G. Polyauriomethane Compounds. *Angew. Chem. Int. Ed. Engl.* **1988**, *27*, 419–421. [CrossRef]
28. Schmidbaur, H. Ludwig Mond Lecture. High-Carat Gold Compounds. *Chem. Soc. Rev.* **1995**, *24*, 391–400. [CrossRef]

29. Jaw, H.-R.C.; Meral Savas, M.; Rogers, R.D.; Mason, W.R. Crystal Structures and Solution Electronic Absorption and MCD Spectra for Perchlorate and Halide Salts of Binuclear Gold(I) Complexes Containing Bridging $Me_2PCH_2PMe_2$(Dmpm) or $Me_2PCH_2CH_2PMe_2$ (Dmpe) Ligands. *Inorg. Chem.* **1989**, *28*, 1028–1037. [CrossRef]
30. Pyykkö, P. Strong Closed-Shell Interactions in Inorganic Chemistry. *Chem. Rev.* **1997**, *97*, 597–636. [CrossRef]
31. Scherbaum, F.; Grohmann, A.; Huber, B.; Krüger, C.; Schmidbaur, H. "Aurophilicity" as a Consequence of Relativistic Effects: The Hexakis(Triphenylphosphaneaurio)Methane Dication $[(Ph_3PAu)_6C]^{2\oplus}$. *Angew. Chem. Int. Ed. Engl.* **1988**, *27*, 1544–1546. [CrossRef]
32. Pyykkö, P. Theoretical Chemistry of Gold. *Angew. Chem. Int. Ed.* **2004**, *43*, 4412–4456. [CrossRef] [PubMed]
33. Dobrzańska, L.; Raubenheimer, H.G.; Barbour, L.J. Borromean Sheets Assembled by Self-Supporting Argentophilic Interactions. *Chem. Commun.* **2005**, 5050–5052. [CrossRef] [PubMed]
34. Chen, C.Y.; Zeng, J.Y.; Lee, H.M. Argentophilic Interaction and Anionic Control of Supramolecular Structures in Simple Silver Pyridine Complexes. *Inorg. Chim. Acta* **2007**, *360*, 21–30. [CrossRef]
35. Liu, X.; Guo, G.C.; Fu, M.L.; Liu, X.H.; Wang, M.S.; Huang, J.S. Three Novel Silver Complexes with Ligand-Unsupported Argentophilic Interactions and Their Luminescent Properties. *Inorg. Chem.* **2006**, *45*, 3679–3685. [CrossRef]
36. Mohamed, A.A.; Pérez, L.M.; Fackler, J.P. Unsupported Intermolecular Argentophilic Interaction in the Dimer of Trinuclear Silver(I) 3,5-Diphenylpyrazolates. *Inorg. Chim. Acta* **2005**, *358*, 1657–1662. [CrossRef]
37. Blessing, R.H. An Empirical Correction for Absorption Anisotropy. *Acta Crystallogr. A* **1995**, *A51*, 33–38. [CrossRef] [PubMed]
38. Sheldrick, G.M. *SADBS Version 2.10 Siemens Area Detector Correction*; Universitaet Goettingen: Goettingen, Germany, 2003.
39. Sheldrick, G.M. *SHELXTL Version 6.1*; Bruker AXS, Inc.: Madison, WI, USA, 2002.
40. Sheldrick, G.M. *GM SHELXS97 and SHELXL97*; Universitaet Goettingen: Goettingen, Germany, 2002.
41. Dolomanov, O.V.; Bourhis, L.J.; Gildea, R.J.; Howard, J.A.K.; Puschmann, H. OLEX2: A Complete Structure Solution, Refinement and Analysis Program. *J. Appl. Crystallogr.* **2009**, *42*, 339–341. [CrossRef]
42. Spek, A.L. Single-Crystal Structure Validation with the Program PLATON. *J. Appl. Crystallogr.* **2003**, *36*, 7–13. [CrossRef]
43. Spek, A.L. Structure Validation in Chemical Crystallography. *Acta Crystallogr. D Biol. Crystallogr.* **2009**, *65*, 148–155. [CrossRef]